J|A|C|S
ARTICLES

Published on Web 11/17/2009

Early Stage Reversed Crystal Growth of Zeolite A and Its Phase Transformation to Sodalite

Heather Greer, Paul S. Wheatley, Sharon E. Ashbrook, Russell E. Morris, and Wuzong Zhou*

EaStChem, School of Chemistry, University of St. Andrews, St. Andrews, Fife KY16 9ST, United Kingdom

Received September 10, 2009; E-mail: wzhou@st-andrews.ac.uk

Abstract: Microstructural analysis of the early stage crystal growth of zeolite A in hydrothermal synthetic conditions revealed a revised crystal growth route from surface to core in the presence of the biopolymer chitosan. The mechanism of this extraordinary crystal growth route is discussed. In the first stage, the precursor and biopolymer aggregated into amorphous spherical particles. Crystallization occurred on the surface of these spheres, forming the typical cubic morphology associated with zeolite A with a very thin crystalline cubic shell and an amorphous core. With a surface-to-core extension of crystallization, sodalite nanoplates were crystallized within the amorphous cores of these zeolite A cubes, most likely due to an increase of pressure. These sodalite nanoplates increased in size, breaking the cubic shells of zeolite A in the process, leading to the phase transformation from zeolite A to sodalite via an Ostwald ripening process. Characterization of specimens was performed using scanning electron microscopy and transmission electron microscopy, supported by other techniques including X-ray diffraction, solid-state NMR, and N_2 adsorption/desorption.

Introduction

According to the classic theory of crystal growth established over 100 years ago, a crystal grows under hydrothermal synthetic conditions from a nucleus, i.e., a bottom-up route.[1] The as-grown crystal morphology is dominated by the slow-growing faces because the fast-growing faces may grow out and not be represented in the final crystal habit, as predicted by the Bravais−Friedel−Donnay−Harker (BFDH) law and Hartman−Perdok approach.[2] However, according to a previous investigation of the crystal growth of zeolite analcime,[3] a perfect polyhedral morphology of the crystal may not be related to the crystal growth rates along different orientations developed from a nucleus. Crystal growth can follow a reversed route, i.e., crystallization starts on the surface of disordered spherical aggregates of nanoparticles to form a crystalline polyhedral shell filled with a disordered core and then extends from the surface to the core. This is the so-called NARS route (nanoparticles, aggregation, surface recrystallization, single-crystal) as first demonstrated in the step-by-step crystal growth of analcime.[3] Soon after, it was found that cubic zeolite A (LTA) particles prepared within a chitosan hydrogel may only contain a very thin crystalline shell, whereas their cores remain amorphous. The amorphous cores can be removed by an acidic treatment, leading to hollow zeolite A boxes.[4] Similar phenomenon of such an aggregation−recrystallization has additionally been observed in other microporous materials, such as cubic $AlPO_4$-11,[5] hollow sodalite (SOD) spheres,[6] and mesoporous materials SBA-15.[7] Furthermore, the aggregation−recrystallization process has also been found in other nonporous hollow spherical particles, e.g., pervoskite $CaTiO_3$,[8] TiO_2,[9] $In(OH)_3$,[10] $Ni(OH)_2$,[11] and even metal nanocrystallites.[12] In the present work, early stage crystal growth of zeolite A was investigated with consideration that this material is one of the most important zeolites, manufactured for ion-exchange,[13] adsorption,[14] and even medical applications[15] in megaton amounts each year.

(1) Ostwald, W. *Lehrbuch der Allgemeinen Chemie*; W. Engelmann, Leipzig, Germany, 1896; Vol. 2, Part 1.
(2) (a) Bravais, A. *Études Cristallographic*; Gauthier-Villars: Paris, 1866. (b) Friedel, M. G. *Bull. Soc. Fr. Mineral. Cristallogr.* **1907**, *30*, 326. (c) Donnay, J. D. H.; Harker, D. *Am. Mineral.* **1937**, *22*, 446. (d) Hartman, P.; Perdok, W. G. *Acta Crystallogr.* **1955**, *8*, 49; 521; 525.
(3) Chen, X. Y.; Qiao, M. H.; Xie, S. H.; Fan, K. N.; Zhou, W. Z.; He, H. Y. *J. Am. Chem. Soc.* **2007**, *129*, 13305.
(4) Yao, J. F.; Li, D.; Zhang, X. Y.; Kong, C. H.; Yue, W. B.; Zhou, W. Z.; Wang, H. T. *Angew. Chem., Int. Ed.* **2008**, *47*, 8397.
(5) Wang, Q.; Chen, G.; Xu, S. *Microporous Mesoporous Mater.* **2009**, *119*, 315.
(6) Han, L.; Yao, J. F.; Li, D.; Ho, J.; Zhang, X. Y.; Kong, C.; Zong, Z. M.; Wei, X. Y.; Wang, H. T. *J. Mater. Chem.* **2008**, *18*, 3337.
(7) Linton, P.; Rennie, A. R.; Zackrisson, M.; Alfredsson, V. *Langmuir* **2009**, *25*, 4685.
(8) Yang, X. F.; Williams, I. D.; Chen, J.; Wang, J.; Xu, H. F.; Konishi, H.; Pan, Y. X.; Liang, C. L.; Wu, M. M. *J. Mater. Chem.* **2008**, *18*, 3543.
(9) Liu, S. J.; Gong, J. Y.; Hu, B.; Yu, S. H. *Cryst. Growth Des.* **2009**, *9*, 203.
(10) Chen, L. Y.; Zhang, Z. D. *J. Phys. Chem. C* **2008**, *112*, 18798.
(11) Buscaglia, M. T.; Buscaglia, V.; Bottino, C.; Viviani, M.; Fournier, R.; Sennour, M.; Presto, S.; Marazza, R.; Nanni, P. *Cryst. Growth Des.* **2008**, *8*, 3847.
(12) Xie, S. H.; Zhou, W. Z.; Zhu, Y. Q. *J. Phys. Chem. B* **2004**, *108*, 11561.
(13) Hui, K. S.; Chao, C. Y. H.; Kot, S. C. *J. Hazard. Mater.* **2005**, *127*, 89.
(14) Moore, T. T.; Koros, W. J. *Ind. Eng. Chem. Res.* **2008**, *47*, 591.
(15) Mowbray, M.; Tan, X. J.; Wheatley, P. S.; Morris, R. E.; Weller, R. B. *J. Invest. Dermatol.* **2008**, *128*, 352.

10.1021/ja907475z

Although a core−shell structure after surface crystallization was found in zeolite A synthesized in the presence of chitosan,[4] the microstructures of the specimens before and after the crystallization have not yet been investigated. There is another long-standing problem during the synthesis of zeolite A, i.e., with extended reaction times under the constant synthetic conditions, the phase of zeolite A would fully transform to sodalite. Subotic et al. proposed, mainly from powder X-ray diffraction (PXRD) results, that the transformation included several steps: dissolution of zeolite A particles, supersaturation of the liquid phase with aluminosilicate ions, nucleation of hydroxyl-sodalite from the solution, and crystal growth of sodalite.[16] However, the details of this phase transformation are still not fully understood to date. Herein, we report our recent investigation of the early stage crystal growth of zeolite A and a new phase transformation mechanism from zeolite A to SOD within the polymer networks of the un-cross-linked biopolymer chitosan hydrogel.

Experimental Section

The synthetic method for zeolite A was the same as previously reported where biopolymer chitosan was employed as a non-structure-directing agent.[4] In a typical procedure, 7 cm^3 of acetic acid (Fisons, 1 M) was mixed with 14 cm^3 of distilled water in a polypropylene bottle. An amount of 1.2 g of chitosan (low or high molecular weight, Aldrich) was gradually dissolved in the prepared acidic solution under magnetic stirring for 1 h, followed by addition of 3.38 g of colloidal silica (LUDOX HS-30, 30 wt %, Aldrich) to give a homogeneous gel. The alkaline solution was prepared by mixing 5 g of NaOH (Fisher) and 2.45 g of sodium aluminate (Riedel-de Haën) with 20 cm^3 of distilled water. The solution was stirred for 0.5−1 h until it became clear. The $Na_2O/Al_2O_3/H_2O$ alkaline solution was added to the chitosan/acetic acid/silica solution without stirring, resulting in a sodium aluminosilicate gel entrapped inside the chitosan hydrogel. This gel was sealed and aged at room temperature for 18 h. The gel was then put in an oven for hydrothermal treatment at 90 °C. The reaction was stopped after 0.5, 1, 2, 3, 4, 6, 22, 72, and 168 h, respectively. The sample was washed repeatedly with distilled water until pH of less than 8 was attained, followed by drying at 90 °C overnight.

The chitosan biopolymer was removed by treatment with acetic acid solution (Fisons, 0.1 M). If the concentration of the acid is too high, e.g., 0.35 M, a large part of the zeolite A crystals are destroyed. The template can also be removed by calcination, e.g., at 550 °C in air. However, calcination may cause further crystallization (Figure S1 in the Supporting Information). The products obtained using the biopolymer chitosan hydrogel with a low molecular weight and a high molecular weight were compared. Both products look similar, except that the crystallinity of the product using a high molecular weight template was relatively low when other conditions were the same.

The final specimens were designated LTA(*X*), where *X* stands for reaction time in hours. For a comparison, the standard method for the synthesis of zeolite A without using chitosan according to the literature procedure[17] was also used to synthesize a monophasic zeolite A sample, designated LTA(standard).

Initial characterization of the specimens was performed using PXRD on a Philips diffractometer using Cu Kα radiation operating in Bragg−Brentano geometry. Slow-scanning PXRD data were collected on a STOE STADIP diffractometer in Debye−Scherrer geometry using 0.5 mm quartz capillaries over a period of 15 h. Morphology of the specimens were examined by using scanning electron microscopy (SEM) on a Jeol JSM-5600 microscope operating at 20−30 kV equipped with an Oxford INCA system for energy-dispersive X-ray spectroscopy (EDX). The powder samples for SEM were coated with Au in order to reduce the beam charging. Selected area electron diffraction (SAED) patterns, transmission electron microscopic (TEM), and high-resolution transmission electron microscopic (HRTEM) images were obtained on a Jeol JEM-2011 electron microscope, also equipped with an EDX system, operating at 200 kV.

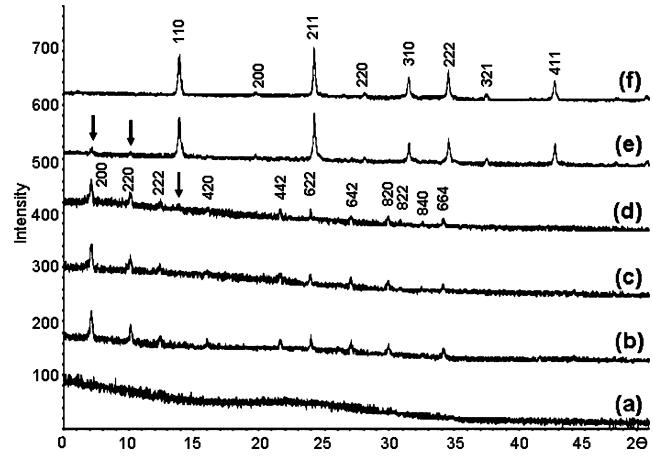

Figure 1. PXRD pattern of samples prepared with different times of hydrothermal treatment: (a) 0.5, (b) 1, (c) 4, (d) 22, (e) 72, and (f) 168 h. Patterns d and f are indexed to zeolite A and sodalite structures, respectively. The chitosan was removed by 0.1 M acetic acid treatment. The arrow in pattern d indicates a weak diffraction peak of sodalite, and the two arrows in pattern e mark diffraction peaks from zeolite A.

For examination of the porosity of the products, the Brunauer−Emmett−Teller (BET) surface area and the pore volume were measured by N_2 adsorption/desorption isotherms at −196 °C on a Micromeritics ASAP 2020. Since the pores in the as synthesized zeolite Na-A were not accessible to N_2, cation exchange of Na^+ by Ca^{2+} was carried out.[18] Ca^{2+}-exchanged zeolite A samples were prepared by dispersing 2 g of the zeolite in a 70 cm^3 solution of calcium acetate hydrate (Fisons, 97% min, 1 M) and stirring for 4 h. The product was recovered by filtration, washed with distilled water, followed by drying at 90 °C overnight. Elemental analysis was carried out using a Agilent 7500 series inductively coupled plasma mass spectrometer (ICP-MS) equipped with laser ablation.

^{29}Si NMR spectra were acquired using a Bruker Avance III 600 spectrometer, equipped with a wide-bore 14.1 T magnet, at a Larmor frequency of 119.2 MHz. Samples were packed into conventional 4 mm ZrO_2 rotors and rotated at a rate of 10 kHz. A recycle interval of 20 s was employed. Chemical shifts are recorded in ppm, relative to TMS(aq), via a secondary solid reference of forsterite at −62 ppm.

Results and Discussion

The PXRD patterns of the specimens with different reaction times are shown in Figure 1. After a reaction time of 0.5 h the sample LTA(0.5) appears to be amorphous. When the reaction time is extended beyond 1 h weak diffraction peaks characteristic of zeolite A begin to appear in the PXRD pattern. These characteristic zeolite A PXRD peaks remained present throughout the 4 and the 22 h reaction times. Most observed peaks can be indexed to the face-centered cubic (fcc) unit cell with dimensions $a = 24.61$ Å, matching the standard structural data (space group $Fm3\bar{c}$) published by International Zeolite Associa-

(16) Subotic, B.; Skrtic, D.; Smit, I.; Sekovanic, L. *J. Cryst. Growth* **1980**, *50*, 498.

(17) Robson, H., Lillerud, K. P., Eds. *Verified Synthesis of Zeolitic Materials*; Elsevier: Amsterdam, The Netherlands, 2001.

(18) Rakoczy, R. A.; Traa, Y. *Microporous Mesoporous Mater.* **2003**, *60*, 69.

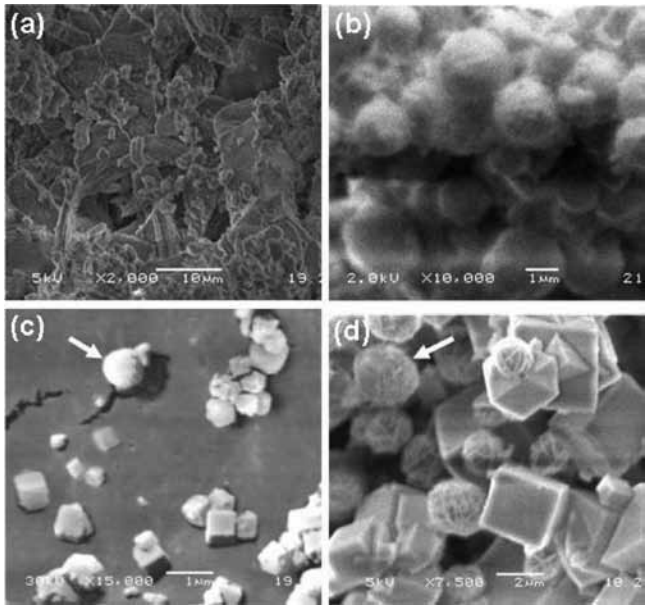

Figure 2. SEM images from specimens of crystal growth for zeolite A with different reaction times: (a) 0.5 h, (b) 1 h (using high molecular weight chitosan), (c) 1 h (using low molecular weight chitosan), and (d) 4 h. Low molecular weight chitosan was used for samples in panels a and d. The arrow in panel c indicates a spherical particle, and that in panel d points to a particle with half cubic LTA and half thread-ball-like SOD.

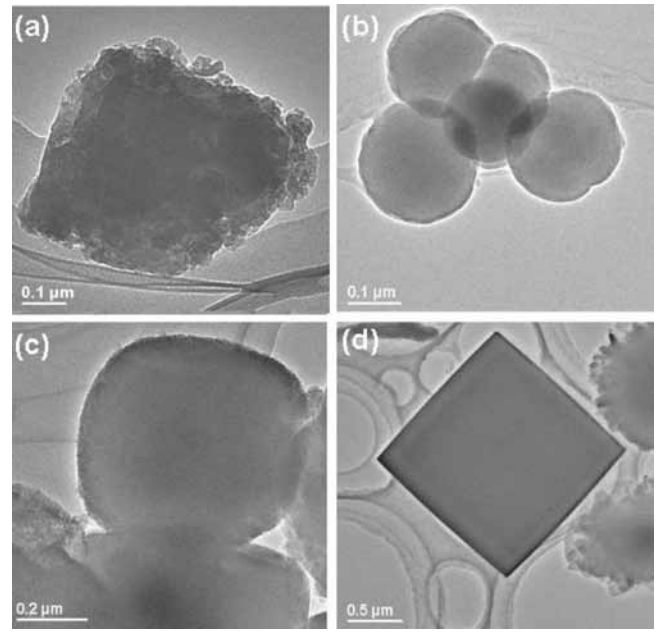

Figure 3. TEM images of the specimens with different reaction times: (a) 0.5, (b and c) 1, and (d) 3 h.

tion.[19] Closer examination of the PXRD pattern from sample LTA(22) revealed a minor impurity phase started to crystallize with the characteristic PXRD pattern of sodalite. When the hydrothermal treatment is increased from 1 h through to 22 h, the diffraction peaks of zeolite A gradually became sharper indicating that the crystallinity of zeolite A increases with increasing reaction time.

The PXRD pattern of LTA(72) contains mainly sodalite with a small content of zeolite A. The sample LTA(168) contains almost phase pure sodalite as all the observed diffraction peaks can be indexed to a body-centered cubic (bcc) unit cell with dimension $a = 8.848$ Å (space group $Im\bar{3}m$), which is similar to the primitive structure previously reported (space group $P\bar{4}3n$)[19] with the off-bcc diffraction peaks, such as (210), (320), (410), etc., missing.

Some extraordinary phenomena were observed in the SEM and TEM images. No regularly shaped particles were found in the specimen after hydrothermal treatment for 0.5 h (Figure 2a). TEM images from this sample also confirmed a noncrystalline property and an irregular morphology of particles (Figure 3a). No diffraction spots were observed on the SAED patterns from this sample, in agreement with the PXRD results (Figure 1a). It is obvious that, at this stage, the precursor and chitosan molecules aggregate without notable crystallization.

After hydrothermal treatment for 1 h, Figure 2b shows the appearance of spherical particles in the SEM image using high molecular weight chitosan which are $1-2$ μm in diameter, similar to the typical size of zeolite A cubes. A small number of cubic particles were also observed. However, SEM image of LTA(1) using low molecular weight chitosan (Figure 2c) displays a substantial increase in the proportion of cubic particles (spherical particles were also present as indicated by an arrow). This effect can be attributed to the viscosities of the resultant hydrogel used in the hydrothermal synthesis. Diffusion of the species involved in crystal growth will be much quicker through the low-viscosity low molecular weight chitosan resulting in quicker crystallization of the first phase to appear (zeolite A). Therefore, low molecular weight chitosan was selected on this basis for further study. A typical TEM image of small spherical particles is shown in Figure 3b with the presence of many larger particles. The spherical particles are noncrystalline in nature. Figure 3c shows a TEM image of a particle having a shape in between spherical and cubic morphologies. No diffraction spots were observed from SAED patterns. However, the appearance of these particles implies possible partial crystallization on the surface as observed in the crystal growth of analcime.[3]

When the reaction time increased to 3 or 4 h, a large number of cubic particles with sharp edges were observed from SEM (Figure 2d) and TEM images (Figure 3d). The cubic particles gave very weak diffraction consistent with the zeolite A structure, which disappeared in less than 1 min under the electron beam irradiation with a normal beam density, indicating that zeolite A crystals were beam-sensitive and decomposed very quickly. In these samples, some thread-ball-like particles are seen, which have no smooth surface as shown in the SEM image in Figure 2d. Two particles on right side of the TEM image in Figure 3d are these thread-ball particles, too. Better quality SEM and TEM images focused on these thread-ball particles can be seen in Supporting Information Figure S2.

The thread-ball particles gave polycrystalline SAED patterns of sodalite, indicating that they are clusters of sodalite nanoplates. Some particles show half cubic and half thread-ball particles as indicated by an arrow in Figure 2d. Bearing in mind that sodalite crystals usually have a dodecahedral morphology, the formation mechanism of these thread-ball-like clusters is of great interest, implying that they were developed in a special environment. The sodalite phase is not detected from PXRD patterns of these samples with the reaction time of 3 and 4 h with the chitosan hydrogel removed by 0.1 M acetic acid treatment (Figure 1c), because the proportion of this phase is very low. However, very weak diffraction peaks of sodalite were

(19) Treacy, M. M. J.; Higgins, J. B. *Collection of Simulated XRD Powder Patterns for Zeolites*, 5th revised ed.; Elsevier: London, 2007.

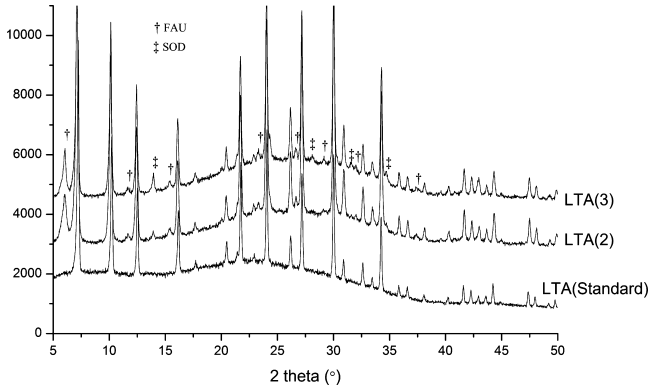

Figure 4. PXRD patterns collected overnight from zeolite LTA(standard) prepared without using biopolymer chitosan and samples LTA(2) and LTA(3) using biopolymer chitosan. The minor phases of zeolite FAU and SOD are indicated.

detected in the PXRD patterns of the samples with the chitosan removed by calcination (Supporting Information Figure S3).

To further confirm the early appearance of the sodalite phase, slow-scanning PXRD patterns were collected overnight for LTA(2) and LTA(3) as well as the sample LTA(standard) prepared without using biopolymer chitosan (Figure 4). The latter sample shows a pure zeolite A phase without any crystalline impurities. Minor phases of faujasite-type zeolite FAU and SOD were detected from LTA(2) and LTA(3). The content of SOD increased significantly from LTA(2) to LTA(3), whereas the change of the faujasite (FAU) phase is not obvious. The very small amount of FAU was believed to have no major inference to the formation of zeolite A and phase transformation from LTA to SOD. It has been noticed that both LTA(2) and LTA(3) contain a large amount of amorphous phase, indicated by a large bump in the background ranging from 15° to 40° 2θ. Another phenomenon is that the diffraction peaks of LTA(standard) are much sharper than those from LTA(2) and LTA(3). For example, the peak widths at half-height of the (200) peak (at about 7° 2θ) are 0.14° for LTA(standard) and 0.22° and 0.16° for LTA(2) and LTA(3), respectively, indicative of a smaller crystal dimension of both LTA(2) and LTA(3). There is a slight increase in sharpness from LTA(2) to LTA(3) as would be expected from longer crystallization times. However, the overall dimensions of the cubes of all three samples are similar ($\sim$2 μm), indicating that the cubes in LTA(2) and LTA(3) are probably core−shell particles as observed previously.[4]

It is surprising to find the capacities of N_2 adsorption of LTA(2) and LTA(3) are comparable to that of LTA(standard) as seen from the N_2 adsorption/desorption isotherms (Supporting Information Figure S4). Surface areas and the total pore volumes are 608.52 m^2/g and 0.2698 cm^3/g in LTA(2), 556.06 m^2/g and 0.2440 cm^3/g in LTA(3), and 654.67 m^2/g and 0.2888 cm^3/g in LTA(standard). It is well-known that zeolite SOD does not adsorb N_2 since the windows of the β-cages are too small. Zeolite A contains both α-cages and β-cages, and only the α-cages can uptake N_2. If all the cubes have the core−shell structure, the high N_2 adsorption capacity of LTA(2) and LTA(3) implies that their disordered cores must be able to adsorb N_2 with a capacity similar to that of zeolite A. The observed hysteresis loops from LTA(2) and LTA(3) indicate the pores in these specimens are not merely micropores but are mixture of micropores and mesopore-like interparticulate spaces, which are more like in the cores of cubes.

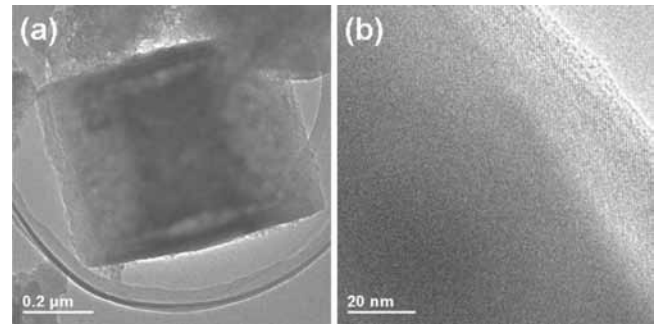

Figure 5. (a) TEM image of cubic zeolite A particle after an electron beam annealing for a few minutes. (b) HRTEM image of a cubic zeolite A particle showing a crystalline shell and amorphous core.

Although HRTEM images of zeolite A have been obtained by many groups since the first report in 1980,[20] it was found that the zeolite A particles with only a thin crystalline shell were much more beam-sensitive. In our previous work, we found several operations might help to stabilize the samples, including drying the specimen, using low irradiation dose, annealing the specimen using electron beam, and using a minimum magnification for HRTEM imaging. Following these operations, we have obtained very good HRTEM images from beam-sensitive samples, such as zeolites,[3,21] C_{60} nanowires,[22] and more recently metal−organic frameworks (MOFs).[23]

In the present work, it was found that, for most zeolite A cubes, the maximum irradiation dose that the samples could tolerate was about 2.0 pA/cm^2. When we reduced the irradiation dose to <2.0 pA/cm^2, the crystal structure could be maintained under the electron beam irradiation for more than 20 min. After annealing cubes of zeolite A using the electron beam with low irradiation dosage, a separation of the surface layer from the core could be observed for a few cubes as shown in Figure 5a. This phenomenon is similar to that previously observed for a zeolite A specimen,[4] except that the surface layer (ca. 30−50 nm) is much thicker. Such a separation was not observed for the majority of cubes in our samples, indicating that the cores of these cubes are quite dense.

HRTEM images revealed a core−shell structure, i.e., a crystalline cubic box with an amorphous core as shown in Figure 5b. The thickness of the crystalline layer in the particle is about 30 nm. The measured *d*-spacing of the lattice fringes is about 8.3 Å, which can match the (220) planes in zeolite A. This core−shell structure is different from single-crystalline cubes of zeolite A, the HRTEM images from the latter showing the lattice fringes across the whole particle (Supporting Information Figure S5).

The chemical compositions of zeolite A and sodalite are very similar, and both have a 1:1 ratio of silicon to aluminum. EDX spectra from cubic and thread-ball particles were almost identical. Fortunately, these two phases have significantly

(20) Bursill, L. A.; Lodge, E. A.; Thomas, J. M. *Nature* **1980**, *286*, 111.
(21) (a) Wright, P. A.; Zhou, W. Z.; Perez-Pariente, J.; Arranz, M. *J. Am. Chem. Soc.* **2005**, *127*, 494. (b) Villaescusa, L. A.; Zhou, W. Z.; Morris, R. E.; Barrett, P. A. *J. Mater. Chem.* **2004**, *14*, 1982. (c) Zhou, W. Z. *J. Mater. Chem.* **2008**, *18*, 5321.
(22) (a) Geng, J. F.; Zhou, W. Z.; Skelton, P.; Yue, W. B.; Kinloch, I. A.; Windle, A. H.; Johnson, B. F. G. *J. Am. Chem. Soc.* **2008**, *130*, 2527. (b) Geng, J. F.; Solov'yov, I. A.; Zhou, W. Z.; Solo'yov, A. V.; Johnson, B. F. G. *J. Phys. Chem. C* **2009**, *113*, 6390.
(23) Xiao, B.; Byrne, P. J.; Wheatley, P. S.; Wragg, D. S.; Zhao, X. B.; Fletcher, A. J.; Thomas, M.; Peters, L.; Evans, J. S. O.; Warren, J. E.; Zhou, W. Z.; Morris, R. E. *Nat. Chem.* **2009**, *1*, 289.

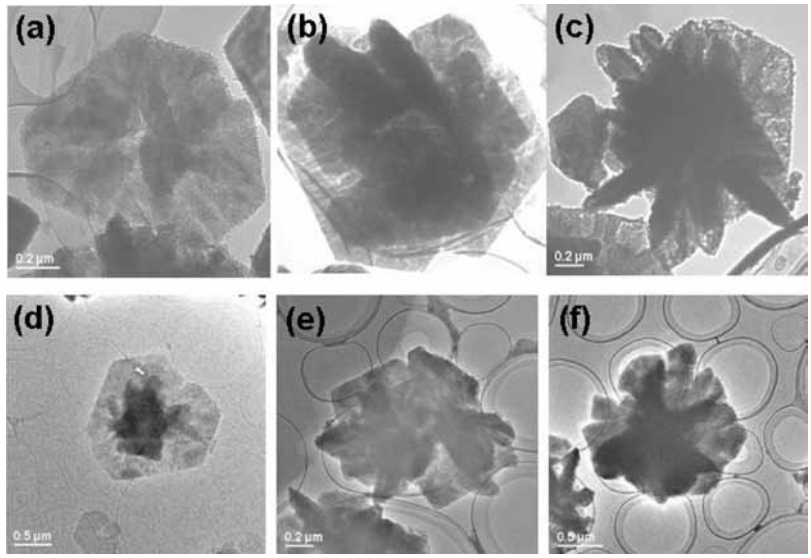

Figure 6. TEM images of individual particles of sodalite nanoplates with evidence of original cubic particles from the samples of (a−c) LTA(72) and (d−f) LTA(168).

different morphologies, cubes for zeolite A and thread-ball particles for sodalite. Therefore, they can be identified easily from either SEM or TEM images. Their structures are also closely related to each other. The framework of zeolite A is built up by β-cages connected by double four-rings (D4R), whereas in sodalite, the β-cages are connected by sharing single four-rings. The mass density of sodalite (2.29 g cm^{-3}) is therefore slightly higher than that of zeolite A (2.00 g cm^{-3}).

When the reaction time was further increased from 4 h, the quantity of cubic zeolite A particles decreased and the quantity of sodalite particles increased as observed from the TEM images, in agreement with the PXRD results. The phase transformation from zeolite A to sodalite has been investigated previously by many groups. For example, Gualtieri et al. found that at higher crystallization temperatures and/or with prolonged heating, zeolite A would be replaced by hydroxyl-sodalite. They also concluded this replacement took place by secondary nucleation of sodalite.[24] A crucial question to ask is how the existing cubes of zeolite A undergo transformation to sodalite step by step. A direct solid-state transformation of zeolite A to sodalite is nearly impossible due to the large energy required to remove D4R from the former. Huang and Havenga performed high-pressure IR spectra and found that zeolite A loses its D4R at 22−28 kbar by observation of the disappearance of the characteristic vibration band at 463 cm^{-1}.[25] It is even more interesting to see that the 463 cm^{-1} band reappeared in the pressure-released spectrum. If nucleation of sodalite occurs separately from that of zeolite A then the consumption of zeolite A crystals via Ostwald ripening should therefore show some intermediate morphologies. On the other hand, the zeolite A samples in the present work have a core−shell structure, and the location of the secondary nucleation of sodalite could be either in the solution or in the amorphous cores of the cubic particles.

Fortunately, particles with partially cubic and thread-ball morphologies, as indicated by an arrow in Figure 2d, increased in the samples with increasing reaction times, allowing us to observe the microstructures of these intermediate morphologies

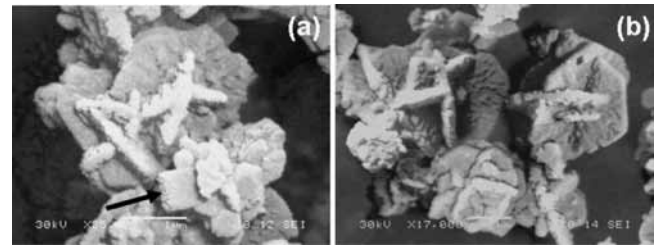

Figure 7. (a) SEM images of LTA(72) containing mainly sodalite but also a few cubic zeolite A particles (indicated by an arrow). (b) SEM images of LTA(168).

between cubic and thread-ball-like particles. Figure 6 shows some of these particles, which look like damaged zeolite A cubes with sodalite nanoplates developed within their centers. The broken cubes do show regular edges, and the cubic morphology is partially maintained in the particle in Figure 6d with some sodalite nanoparticles appearing in the center of the particle. This conclusion was further proved by images through tilting. Very early stage crystal growth of sodalite in the cores of these cubic particles can also been seen in Figure 6a. In other particles in Figure 6, the sodalite crystallites developed further to break the cubic shells of zeolite A. Most of the particles in LTA(72) and LTA(168) are clusters of sodalite nanoplates as shown in Figure 7. However, a small quantity of cubes of zeolite A were still observed from LTA(72) as indicated by an arrow in Figure 7a, whereas no cubic particles were detected in LTA(168) (Figure 7b) as is consistent with the PXRD data (Figure 1).

The above observation of the step-by-step crystal growth allows us to propose a new formation mechanism of zeolite A and a new phase transformation mechanism from zeolite A to sodalite with presence of biopolymer chitosan, summarized in Figure 8. At the very beginning, precursor and chitosan aggregate into irregular particles (step 1). These particles further aggregate into larger amorphous spherical particles (step 2). Surface crystallization then occurs on the surface of the spheres to form a single-crystalline cubic shell of zeolite A. It is assumed that the surface crystallization is similar to that observed from zeolite analcime.[3] Multiple nucleation takes place on the surface of the sphere instead of single nucleation for each sphere, forming many crystalline islands (steps 3). Unfortunately, these

(24) Gualtieri, A.; Norby, P.; Artioli, G.; Hanson, J. *Phys. Chem. Miner.* **1997**, *24*, 191.
(25) Huang, Y. N.; Havenga, E. A. *Chem. Phys. Lett.* **2001**, *345*, 65.

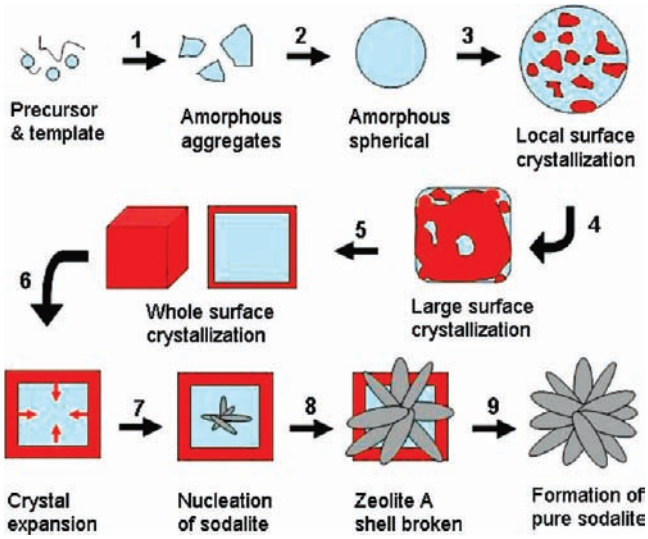

Figure 8. Schematic drawing of a proposed new crystal growth route of zeolite A and the phase transformation from zeolite A to sodalite.

islands were not observed in the present work due to the limitation of resolution of SEM. When the crystalline islands extend on a spherical surface, they fuse together and, more importantly, adjust their orientations (step 4) thus forming six {100} faces of a cubic shell simultaneously via an Ostwald ripening process (step 5). The observed (200) lattice fringes in Figure 5b therefore have a 45° angle with the face of the cube. After the formation of the single-crystalline cubic shell, the crystallization process extends inward to the amorphous core to increase the thickness of the shell (step 6), which is also similar to the case in analcime.[3]

Up to step 6, no appearance of sodalite could be observed. It is obvious that the aggregation is a crucial step, which is enhanced by chitosan. The biopolymer chitosan, $(C_6H_{11})_4N)_n$, contains abundant amino and hydroxyl groups and can bond with active aluminosilicate precursor species to form large aggregates. In the standard synthetic conditions without using a biopolymer, crystal growth of zeolite A would follow the classic route: nucleation−crystal growth, since no disordered aggregates are developed. For the phase transformation from zeolite A to sodalite in a classic crystallization route, the secondary nucleation of sodalite−Ostwald ripening mechanism[24] and the redissolution of zeolite A−nucleation of sodalite mechanism[26] were previously proposed. More accurate crystallization curves for zeolite A and sodalite were produced by Walton et al., using an energy-dispersive XRD method.[27] In the present work, when the core−shell cubes formed, mass transportation across the crystalline shell became difficult. When the crystalline shell extends inward to the amorphous core, the pressure in the core may increase if the core is dense, because the process of crystallization of the core of zeolite A is a process of density decrease. Nucleation of sodalite, having a higher density in comparison with zeolite A, takes place in the amorphous cores of cubic particles where the pressure is built up (step 7). This proposed mechanism is consistent with the previous work on crystal growth under high pressure, for example, the IR experiments by Huang and Havenga[25] implied

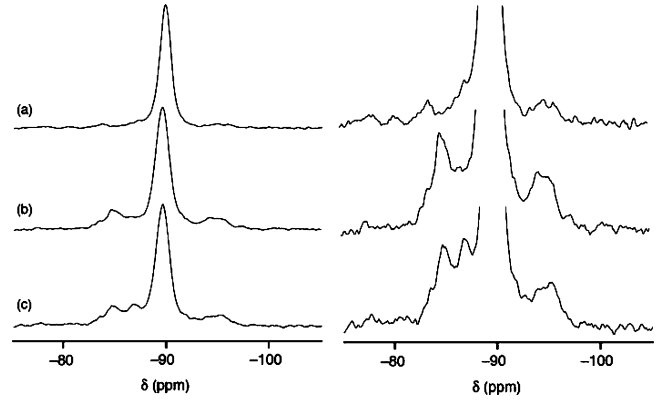

Figure 9. ^{29}Si (119.2 MHz) MAS NMR spectra of (a) LTA(standard) prepared without using biopolymer chitosan and samples prepared using biopolymer chitosan (b) LTA(2) and (c) LTA(3). Spectra are also shown with an expansion of the vertical scale.

that an increased pressure can enhance the formation of sodalite. High-pressure-induced phase transformation from a low-density zeolite to a high-density one was also reported in other zeolite systems, e.g., from ZSM-5 to ZSM-11.[28] Furthermore, it was noticed that sodalite crystals were found to form inside amorphous gel particles as reported by Fan et al.[29]

The sodalite nanoplates expanded in size to break through the zeolite A cubic shells, and finally the consumption of zeolite A occurred through an Ostwald ripening process (step 8). Consequently, under the present synthetic conditions, no pure zeolite A was ever produced at any stage, although reasonably large cubic particles appeared as detected by SEM and TEM. Before true single crystals of zeolite A form, crystals of sodalite start to grow inside the cubic core−shell particles.

To further confirm the complexity of the zeolite A cubes prepared in the present work, solid-state NMR spectra were obtained. Figure 9 shows ^{29}Si (119.2 MHz) MAS NMR spectra of samples LTA(2) and LTA(3), respectively, and LTA(standard) for comparison. In the latter case (Figure 9a), the spectrum is dominated by a peak at −89.8 ppm, typical of Q^4(4 Al) Si species,[30] where the superscript denotes the number of additional bonds formed by the SiO_4 tetrahedron and the number in brackets denotes how many of these species are Al (rather than Si). The SiO_4 tetrahedra appear to form four bonds to four Al species, expected as a result of Lowensteins rule which predicts that links between AlO_4 tetrahedra are rare or absent and Al−O−Al linkages are disfavored.[30] However, the presence of a peak (albeit with much lower intensity) at ∼ −94.5 ppm, attributed to Q^4(3 Al), reveals that the Si/Al ratio is not exactly unity and that a small number of SiO_4 tetrahedra are linked to other Si species. In contrast, the NMR spectra for the samples LTA(2) and LTA(3) show a more complex spectrum, with a number of additional resonances. The Q^4(4 Al) in both cases appears slightly shifted downfield and is also broader, signifying the presence of other Q^4 species with slightly different environments, i.e., some structural disorder. In addition, the appearance of peaks at approximately −85 and −87 ppm indicate the presence of Si species with a lower degree of polymerization, probably Q^3 species. The resonance at −85 ppm is present in

(26) Rios, C. A.; Williams, C. D.; Fullen, M. A. *Appl. Clay Sci.* **2009**, *42*, 446.
(27) Walton, R. I.; Millange, F.; O'Hare, D.; Davies, A. T.; Sankar, G.; Catlow, C. R. A. *J. Phys. Chem. B* **2001**, *105*, 83.
(28) Liu, X.; Su, W.; Wang, Y.; Zhao, X. *Chem. Commun.* **1992**, 902.
(29) Fan, W.; Morozumi, K.; Kimura, R.; Yokoi, T.; Okubo, T. *Langmuir* **2008**, *24*, 6952.
(30) MacKenzie, K. J. D.; Smith, M. E. In *Multinuclear Solid-State NMR of Inorganic Materials*; Pergamon materials series Vol. 6, Elsevier Science Ltd., Oxford, 2002.

both LTA(2) and LTA(3), whereas that at −87 ppm appears only in LTA(3). In this latter sample these resonances contribute approximately 21% of the signal in the spectrum. The presence of these additional peaks suggests structural disorder in the system and is consistent with the appearance of noncrystalline regions within the sample.

Conclusion

On the basis of the present work, we can believe that there are at least two crystal growth routes for zeolite A. One is classic, i.e., the precursor molecules undergo polymerization followed by nucleation and subsequent crystal growth. In this case, aggregation of nanoparticles does not occur and monocrystalline zeolite A is produced, which has been used in many industry processes as a catalyst and, in our own previous research, used as template for producing metal nanowires and metal clusters.[31] The present work demonstrates the second crystal growth route when biopolymer chitosan was added to the synthetic solution. The role of chitosan is to enhance the formation of amorphous aggregates before crystallites grow up. A reversed crystal growth takes place, i.e., crystallization starts on the surface of the amorphous spherical particles and extends to the cores. It is demonstrated again that a characteristic polyhedral shape of zeolite particles is not necessarily an indication of their single-crystal nature. A single-crystalline cubic shell can be developed on surface of amorphous aggregates in the case of zeolite A. When the core−shell structure forms, nucleation of sodalite can occur in the amorphous cores, followed by the crystal growth of sodalite nanoplates and the phase transformation from zeolite A to sodalite via an Ostwald ripening process. This work indicates that the reversed crystal growth route is probably a common phenomenon when aggregation dominates in early stage crystal growth of zeolitic materials and other crystalline solids. A joint research on novel crystal growth routes in some biomimetic materials is currently carried out by two groups at St. Andrews and National Taiwan Universities.

Acknowledgment. W.Z. thanks the Royal Society and University of St. Andrews for financial support. The authors also thank Mr. Ross Blackley for his assistance in SEM and TEM experiments, Mrs. Sylvia Williamson for gas adsorption/desorption experiments, and Paul Wright for helpful discussions. R.E.M. holds a Royal Society Wolfson Research Merit Award. S.E.A. thanks EPSRC for financial support (NMR equipment).

Supporting Information Available: Extra XRD patterns, more detailed SEM and TEM images of sodalite particles, N_2 adsorption/desorption of specimens, and HRTEM images of normal zeolite LTA. This material is available free of charge via the Internet at http://pubs.acs.org.

JA907475Z

(31) (a) Edmondson, M. J.; Zhou, W. Z.; Seiber, S.; Gameson, I.; Anderson, P. A.; Edwards, P. P. *Adv. Mater.* **2001**, *13*, 1608. (b) Readman, J. E.; Barker, P. D.; Gameson, I.; Hriljac, J. A.; Zhou, W. Z.; Edwards, P. P.; Anderson, P. A. *Chem. Commun.* **2004**, 736.